Inorganic Chemistry

Article

pubs.acs.org/IC

Mechanism of Pd-Catalyzed Decarbonylation of Biomass-Derived Hydrocinnamic Acid to Styrene following Activation as an Anhydride

Manuel A. Ortuño,* Büşra Dereli, and Christopher J. Cramer*

Department of Chemistry, Chemical Theory Center, and Supercomputing Institute, University of Minnesota, Minneapolis, Minnesota 55455, United States

Supporting Information

ABSTRACT: All elementary steps in the mechanism of Pd-catalyzed decarbonylation of hydrocinnamic acid through formation of a mixed anhydride species have been characterized through electronic structure calculations. Oxidative addition of the mixed anhydride to a singly or doubly ligated Pd is followed by decarbonylation, alkene formation, and catalyst regeneration. Metal-assisted deprotonation of the alkyl-Pd species by a coordinated carboxylate is predicted to be the rate-determining step; theory suggests that bulkier phosphine ligands (e.g., P(*o*-Tol)$_3$) reduce the free energy of activation substantially, while variation of the auxiliary anhydride has little influence on efficiency.

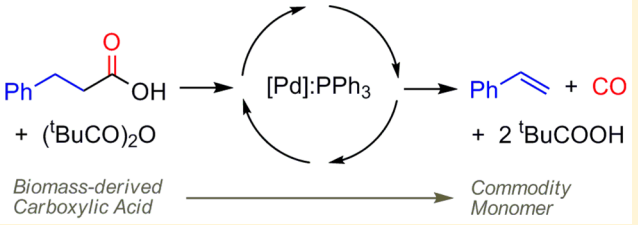

INTRODUCTION

Conversion of natural-product feedstocks into valuable synthetic chemicals has become a crucial issue due to the increasing shortage of fossil reserves.[1,2] Among the different renewable resources available, biomass-derived carboxylic acids are excellent substrates from which to obtain high-value linear α-olefins via catalytic deoxygenation processes (especially those with an odd number of carbon atoms).[3−5]

There is thus considerable interest in the development of convenient methods to facilitate production of such high value products using a sustainable catalytic platform. In particular, decarbonylation/dehydration provides a relevant route to convert readily available carboxylic acids to olefins (Scheme 1a). This process can be catalyzed by transition-metal complexes under homogeneous conditions.[6] While unactivated carboxylic acids are at best weakly reactive,[7] considerably improved results are obtained when a sacrificial anhydride is used (Scheme 1b). Activation of carboxylic acids via anhydrides has been well-described in the literature for other reactions,[8] particularly by the groups of Yamamoto[9] and Goossen.[10] Focusing on decarbonylation processes, Miller et al. initially reported the transformation of fatty acids into terminal alkenes in the presence of Pd and Rh catalysts using acetic anhydride at high temperatures (Scheme 1b).[11,12] While undesired isomerization of internal alkenes occurred with acetic anhydride, Goossen et al.[13] found alternative protocols involving pivalic anhydride to improve selectivity. Most of the work in this area has involved Pd-based catalysts and has focused on the design of protocols with high efficiency under mild reaction conditions,[13−16] in some instances exploiting the reaction to reveal a vinyl group at a late stage in a complex synthesis.[17] Other transition metals known to catalyze this process include Fe[18] and Ir.[19] As an alternative to anhydride coreactants, *p*-nitrophenylester derivatives have shown promising results.[20,21] However, full suppression of isomerization to generally more thermodynamically stable internal alkenes remains a challenge.

With a focus on sustainability, we are interested in the conversion of biomass to produce commodity monomers. Thus, we focus here on a particular system reported by Hillmyer, Tolman, and co-workers that produces styrene in good yields from biomass-derived hydrocinnamic acid and pivalic anhydride at 190 °C in the presence of $PdCl_2$ and PPh_3 (Scheme 2).[15] The effectiveness of the process depends on the anhydride coreactant as well as the [Pd] catalyst.

The currently accepted reaction mechanism following the formation of the mixed anhydride consists of (i) oxidative

Scheme 1. (a) General and (b) Transition-Metal-Catalyzed Anhydride-Mediated Decarbonylation of Carboxylic Acids

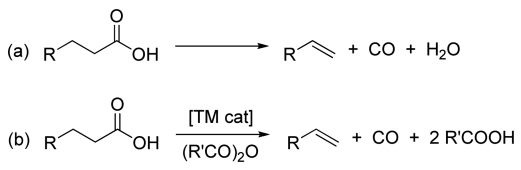

Scheme 2. Pd-Catalyzed Decarbonylation of Hydrocinnamic Acid with Pivalic Anhydride as the Coreactant[15]

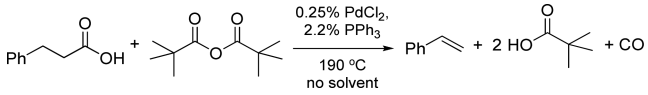

Received: November 17, 2015
Published: April 14, 2016

DOI: 10.1021/acs.inorgchem.5b02664
Inorg. Chem. 2016, 55, 4124−4131

addition, (ii) decarbonylation, (iii) β-hydride elimination, and (iv) catalyst regeneration to yield the product olefin (Figure 1).[6,13,15,18,19] We apply computational electronic structure

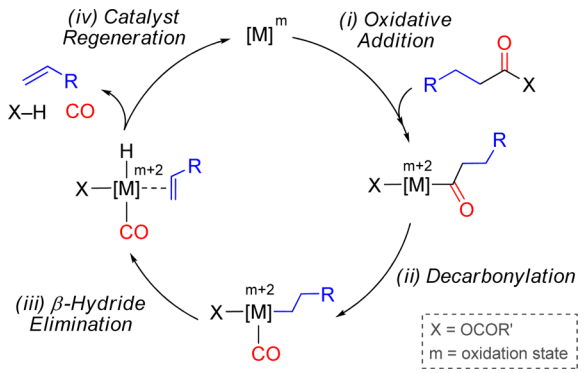

Figure 1. Proposed mechanism for the transition-metal-catalyzed anhydride-mediated decarbonylation.

theory, and in particular density functional theory (DFT),[22] to gain detailed atomistic insights not readily assessed experimentally for individual elementary steps in the mechanism with the goal of contributing to the rational design of better catalysts and experimental conditions. Various reaction pathways have been evaluated at the DFT level, and a number of anhydrides and phosphine ligands with different electronic and steric properties are evaluated and discussed.

COMPUTATIONAL DETAILS

All calculations were performed at the DFT level[23] using the M06-L local density functional[24,25] as implemented in Gaussian 09.[26] This functional accounts for dispersion interactions[25] and performs well in transition-metal chemistry[25,27] and PPh_3 binding enthalpies.[28] An ultrafine grid was used to perform numerical integrations. An automatic density-fitting set generated by the Gaussian program was used to reduce computational expense. For geometry optimizations, the following double-ζ basis sets (DZ) were used: the Stuttgart effective core potential and its associated basis set (SDD) for Pd[29] and the 6-31G(d,p) basis set for H, C, N, O, F, and P,[30] including diffuse functions for O and F atoms.[31] All geometries were fully optimized in the gas phase. The natures of all intermediates and transition states were confirmed by analytic computation of their vibrational frequencies at 463.15 K (the temperature of corresponding experiments[15]). Transition-state (TS) structures were verified to connect with reactants and products by following normal modes associated with the corresponding imaginary frequencies. All frequencies below 50 cm^{-1} were replaced by 50 cm^{-1} when computing vibrational entropies.[32]

The decarbonylation process under study is a solvent-free reaction.[15] The environment of the experimental mixture is difficult to reproduce computationally, but one species must be selected as a solvent for the modeling. As discussed below, the first step of the process is the reaction of hydrocinnamic acid with pivalic anhydride. This process produces an intermediate mixed anhydride that enters the catalytic cycle and liberates one molecule of pivalic acid to the medium. Additionally, another molecule of pivalic acid is released at the end of the catalytic cycle. Therefore, it is reasonable to assign a carboxylic acid compound as a consistent solvent through the global process (hydrocinnamic acid at the very beginning of the reaction and pivalic acid afterward). With respect to the calculations, butanoic acid (BA, $\varepsilon = 2.85$)[33] was used as a model solvent to mimic pivalic acid ($\varepsilon = 2.98$)[33] because the latter is not specifically parametrized. For single-point calculations in solution, the following triple-ζ basis sets (TZ) were used: the Stuttgart effective core potential and its associated basis set (SDD),[29] including one f-polarization function,[34] for Pd and the 6-311++G(d,p) basis set for H, C, N, O, F, and P.[30,31,35] Final Gibbs energies in solution were computed through the addition of Gibbs energy contributions in the gas phase (DZ level) to single-point calculations in butanoic acid (TZ level) using the SMD model.[36] For all species but CO (gas at 1 atm), a factor of $RT \times \ln(24.46)$ was added to account for the 1 atm to 1 M standard-state change. All Gibbs energies in BA solution (ΔG_{BA}) are reported in kcal mol^{-1}.

Finally, the influence of the basis set, solvation during optimization, and density functionals were inspected. DLPNO-CCSD(T) calculations,[37] as implemented in ORCA software,[38] were also performed on a model system to benchmark DFT results (see the Supporting Information for details). These calculations show an agreement with M06-L for the average energies of various stationary points to within ca. 1 kcal mol^{-1} and provide additional validation for the selection of this density functional model.

RESULTS AND DISCUSSION

The reaction conditions of the Pd-catalyzed conversion of hydrocinnamic acid **1** to styrene are shown in Scheme 2. It is well-established that some Pd(II) reagent is first reduced to the Pd(0) species prior to the start of catalysis.[39] Because the ratio between the starting [Pd] and phosphine ligand is ca. 1:9, the well-known and stable $[PdL_4]$ complex **C4** (L = PPh_3) is a reasonable thermodynamic sink for Pd.[40] We thus take the sum of hydrocinnamic acid **1**, pivalic anhydride, and **C4** to be the zero of energy for our discussion of catalysis. Unless stated otherwise, all ΔG_{BA} values correspond to Gibbs energies in a butanoic acid solvent (as a model for pivalic acid) at 463.15 K.

Reaction Mechanism. The computed reaction mechanism is shown in Figure 2. Initially, the hydrocinnamic acid **1** reacts

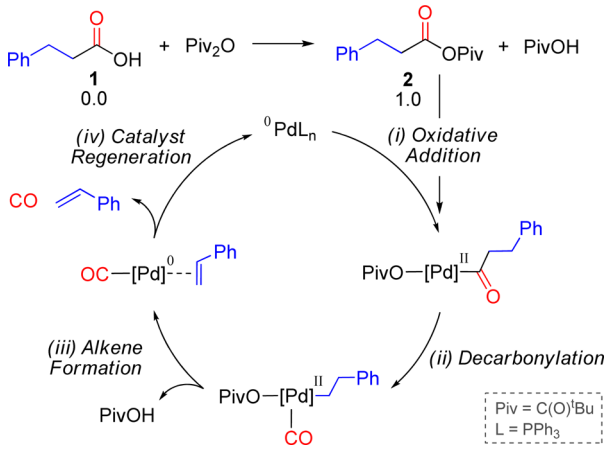

Figure 2. Computed reaction mechanism for the Pd-catalyzed decarbonylation of hydrocinnamic acid **1**. ΔG_{BA} is in kcal mol^{-1}.

with pivalic anhydride to form the mixed anhydride **2** and pivalic acid (a step that is endergonic by 1.0 kcal mol^{-1}). Subsequently, **2** enters the catalytic cycle, which can be divided into four main steps: (i) oxidative addition, (ii) decarbonylation, (iii) alkene formation, and (iv) catalyst regeneration. Each step is independently discussed below.

Oxidative Addition. The first step of the mechanism entails C−O bond breaking of anhydride **2** via oxidative addition at the Pd center (Scheme 3).[9,10] The mixed anhydride **2** has two possible C−O bonds to break, i.e., C−OC(O)^{t}Bu and C(O)O−^{t}Bu. We initially focus on the former bond-breaking mode, which is responsible for the final product styrene. We note that DFT calculations on the analogous oxidative additions of anhydrides have previously been reported by

DOI: 10.1021/acs.inorgchem.5b02664
Inorg. Chem. 2016, 55, 4124−4131

Scheme 3. Oxidative Addition (Step (i))[a]

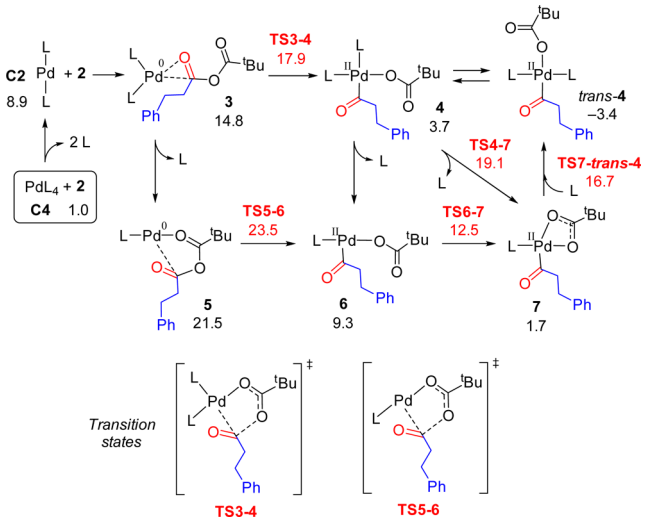

[a]ΔG_{BA} in kcal mol^{-1}.

Goossen et al. as well.[41] Initially, two phosphine ligands must be released from the initial catalyst [PdL_4] **C4** to form the active species [PdL_2] **C2** at 8.9 kcal mol^{-1}. Anhydride **2** can coordinate to **C2** through one of the carbonyl groups to form **3**, which has an energy 14.8 kcal mol^{-1} higher than that of the separated educts. Oxidative addition can take place via **TS3−4**, which has a free energy of 17.9 kcal mol^{-1}, affording the acyl-Pd species **4**. The *cis*-positioned phosphine ligands in **4** (3.7 kcal mol^{-1}) can subsequently rearrange to a much more stable *trans* configuration (*trans*-**4**, −3.4 kcal mol^{-1}).[9a] The isomerization process from **4** may take place through two different pathways: (i) associative substitution via **TS4−7** (19.1 kcal mol^{-1}) to form **7** or (ii) dissociative substitution of one phosphine to form the three-coordinate T-shaped[42] species **6**, which pivalate ligand easily rearranges from the κ^1 to κ^2 coordination mode via **TS6−7** (12.5 kcal mol^{-1}). In either case, the resulting species **7** binds one phosphine ligand via **TS7**-*trans*-**4** (16.7 kcal mol^{-1}).

On the basis of previous studies on related C−O oxidative addition processes, we also considered the participation of monophosphine species.[41b,43,44] At the experimental temperature (463.15 K), the liberation of a phosphine ligand from **3** appears plausible, giving rise to **5**, which has a free energy of 21.5 kcal mol^{-1}. The monophosphine TS structure for oxidative addition, **TS5−6**, has a free energy of 23.5 kcal mol^{-1} and produces coordinatively unsaturated intermediate **6**. As mentioned above, **6** evolves via **TS6−7** to coordinate the pivalate ligand in a κ^2 fashion, forming **7** (1.7 kcal mol^{-1}). Reincorporation of a phosphine ligand via **TS7**-*trans*-**4** (16.7 kcal mol^{-1}) leads to *trans*-**4**.

Previous literature suggests that anionic species can facilitate the oxidative addition of anhydrides.[41] Therefore, we studied the oxidative addition of **2**, including one explicit molecule of pivalate, to form the anionic complex [PdL_2(OPiv)]$^-$ **C2−A** (14.8 kcal mol^{-1}). The corresponding transition state **TS3−4−A** is found, however, at 23.5 kcal mol^{-1}, i.e., 5.6 kcal mol^{-1} above the neutral counterpart **TS3−4**.

Additionally, we explored an alternative C−O bond-breaking process involving the bis-phosphine species. The precomplex **3−Piv** (17.2 kcal mol^{-1}) shows the anhydride bound to Pd via the C(O) of the pivalate moiety. The transition state **TS3−4−Piv** is found at 22.0 kcal mol^{-1}, that is, 4.1 kcal mol^{-1} above **TS3−4**. Because this oxidative addition pathway is less-favored and does not produce the experimentally observed styrene product, no further steps were investigated.

Decarbonylation. After the oxidative addition, a decarbonylation (CO deinsertion) process is proposed to break the C−C(O) bond of the acyl moiety, forming CO and an alkyl-Pd species (Scheme 4).[45] This step is assumed to take place from **7**

Scheme 4. Decarbonylation (Step (ii))[a]

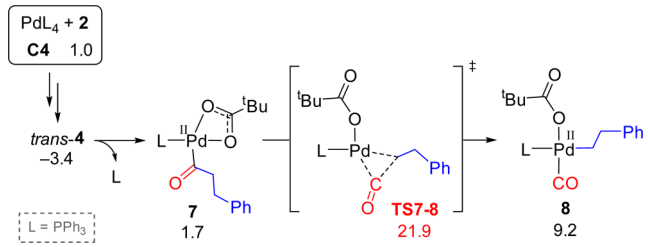

[a]ΔG_{BA} in kcal mol^{-1}.

as the pivalate ligand changing from κ^2 to κ^1 generates a coordination site for the new CO ligand. The CO deinsertion TS structure **TS7−8** has a free energy of 21.9 kcal mol^{-1}, which leads to the alkyl complex **8** at 9.2 kcal mol^{-1}.[46]

Alkene Formation. The alkyl-Pd species **8** can be transformed into the alkene (styrene) product via different reaction pathways (Scheme 5). A direct β-hydride elimination process

Scheme 5. Alkene Formation (Step (iii))[a]

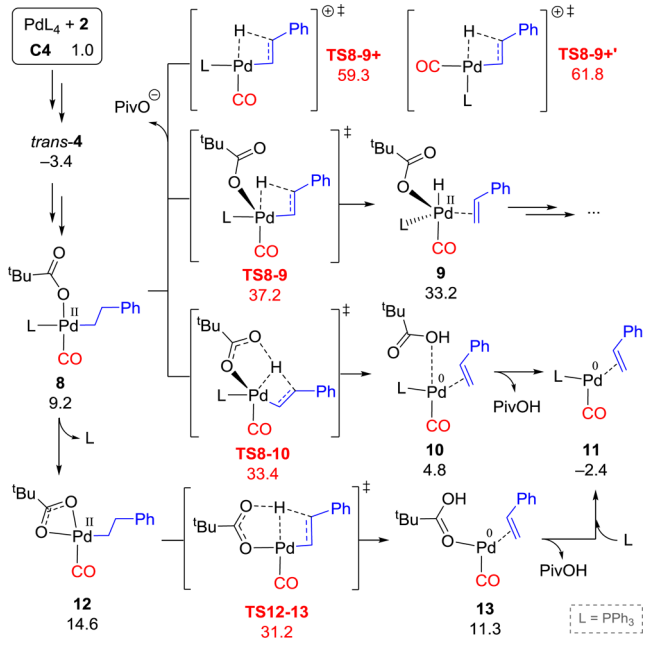

[a]ΔG_{BA} in kcal mol^{-1}.

(Figure 1) is available through **TS8−9** which has a free energy of 37.2 kcal mol^{-1} and delivers a five-coordinate Pd(II) hydride species **9** (33.2 kcal mol^{-1}).[47,48] Alternatively, the loss of pivalate leading to cationic species was also considered. The corresponding cationic β-hydride elimination transition states **TS8−9+** and **TS8−9+′** are found at 59.3 and 61.8 kcal mol^{-1}, respectively. The charge separation process is not favored due to the relatively low polarity of the solvent (ε = 2.85). This

DOI: 10.1021/acs.inorgchem.5b02664
Inorg. Chem. 2016, 55, 4124−4131

pathway may, however, be envisaged when using more polar solvents such as DMPU.[13,21]

As the carboxylate ligand may act as an internal base,[49] we found an alternative intramolecular deprotonation TS structure involving pivalate (**TS8−10**) at 33.4 kcal mol^{-1}. In this TS, the noncoordinated oxygen from the pivalate abstracts the proton from the alkyl ligand, skipping the transient hydride intermediates and forming the Pd(0) species **10** (4.8 kcal mol^{-1}). Further release of the loosely bound pivalic acid gives rise to **11** (−2.4 kcal mol^{-1}). Finally, the phosphine-free species **12**, obtained by removal of the last phosphine ligand in **8**, was also considered.[21] The corresponding deprotonation TS structure **TS12−13** is predicted to have a free energy of 31.2 kcal mol^{-1}; i.e., this pathway is predicted to be more favorable than either of those associated with TS structures **TS8−9** and **TS8−10**. The resulting product **13** (11.3 kcal mol^{-1}) can then exchange pivalic acid for phosphine to arrive at the more stable complex **11**.

Deprotonation TS structures **TS8−10** and **TS12−13** are shown in Figure 3. Interestingly, in each case the Pd center

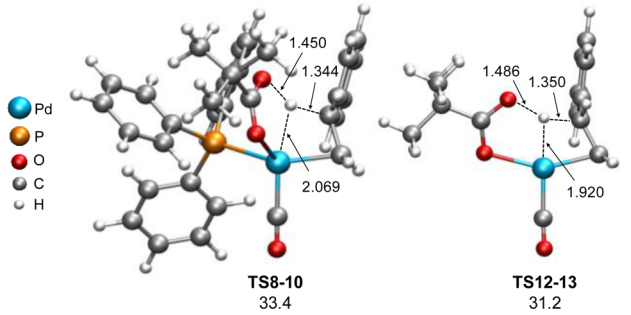

Figure 3. Optimized TS structures **TS8−10** and **TS12−13**. Bond distances are in Å, and ΔG_{BA} is in kcal mol^{-1}.

actively participates in the proton transfer, as judged by the Pd···H distances of 2.069 and 1.920 Å in the two TS structures, respectively.[50]

Catalyst Regeneration. The final step involves regeneration of the catalyst by release of styrene and CO (Scheme 6). From

Scheme 6. Catalyst Regeneration (Step (iv))[c]

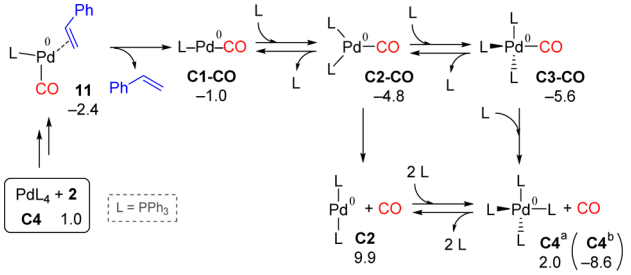

[a]P(CO) = 1 atm. [b]P(CO) = 10^{-5} atm. [c]ΔG_{BA} in kcal mol^{-1}.

11, the styrene product is liberated, forming the species **C1−CO** (−1.0 kcal mol^{-1}). Up to two additional phosphine ligands coordinate to Pd, producing **C2−CO** and **C3−CO**. These [Pd(CO)] complexes are close in Gibbs energy, ca. 5 kcal mol^{-1} below that of the original reactants.[51] Eventually, CO must decoordinate from Pd to regenerate the initial catalyst **C2**.[52] The final energies of the products and reactants were found to be 9.9 and 2.0 kcal mol^{-1} for regeneration of **C2** and **C4**, respectively.

While these values appear to indicate an endergonic reaction, which is not expected to be catalytic, one must note that the calculations employ a standard-state pressure of 1 atm for CO, but experimentally, CO is purged from the reaction as it is produced. When an arbitrary pressure of 10^{-5} atm for CO to mimic the experimental conditions is considered, the reaction becomes clearly exergonic; i.e., **C4** and CO are found at an energy 8.6 kcal mol^{-1} below that of the initial reactants. This value is in agreement with experiments where vigorous bubbling associated with the loss of CO has been reported.[15] Thus, irreversible removal of CO acts as a driving force for the catalysis.

Reaction Profile. The prior results are combined in a Gibbs free-energy reaction coordinate in Figure 4 (the Gibbs free-energy reaction coordinate in the gas phase is located in the Supporting Information). The oxidative addition of **2** to **C2** via **TS3−4** has an activation free energy of 17.9 kcal mol^{-1} above that of **C4**. The resulting bis- and monophosphine acyl derivatives *trans*-**4** and **7** are stable intermediates at −3.4 and 1.7 kcal mol^{-1}, respectively. Subsequent decarbonylation takes place via **TS7−8** with an activation free energy of 25.3 kcal mol^{-1} above that of *trans*-**4**. For the alkene formation process, the metal-assisted deprotonation processes via **TS8−10** and **TS12−13** are the most favored pathways at energies of 36.8 and 34.6 kcal mol^{-1}, respectively, above that of *trans*-**4**. After the loss of styrene, **C3−CO** appears as the most stable Pd(CO) complex at −5.6 kcal mol^{-1}. CO and ligand release from **C3−CO** to **C2** demands 15.5 kcal mol^{-1} (under 1 atm standard-state conditions). Finally, the Gibbs energy of the reaction ΔG_r is −8.6 kcal mol^{-1} (CO pressure of 10^{-5} atm).

To estimate the overall Gibbs energy barrier of the entire catalytic cycle, we need to identify the rate-determining transition state (RDTS) and the rate-determining intermediate (RDI).[53] It is clear that the alkene formation via **TS12−13** is the turnover-limiting step. Regarding the RDI, both *trans*-**4** and **C3−CO** are stable species (i.e., possible resting states). The predicted barrier from *trans*-**4** is 34.6 kcal mol^{-1} (ΔG(**TS12−13**) − ΔG(*trans*-**4**)), whereas the predicted barrier from **C3−CO** is 28.2 kcal mol^{-1} (ΔG(**TS12−13**) − ΔG(**C3−CO**) + ΔG_r). Therefore, although **C3−CO** is the most stable species, the overall barrier is estimated from *trans*-**4** to **TS12−13**, resulting in 34.6 kcal mol^{-1}. At 463.15 K, this turnover-limiting activation free energy is consistent with the experimental conditions.

The present mechanism (i.e., a C−H bond-breaking process as the rate-determining step) suggests that a strong kinetic isotope effect[54] should be observed for the primary hydrogen. The computed Gibbs energy barriers from *trans*-**4** to **TS12−13** for hydrogen and deuterium are 34.6 and 35.7 kcal mol^{-1}, respectively. With the exclusion of tunneling and anharmonicity, the computed kinetic isotope effect (KIE)[55] is thus 3.3 at 463.15 K.

Catalysis Using Pd−CO Species. While the release of CO forms **C2** and **C4** and thereby initiates a new catalytic cycle, a subsequent reaction may hypothetically start from **C1−CO** instead. In this case, because CO is not removed, the rate-determining intermediate is now **C3−CO** (instead of *trans*-**4**). After the loss of two phosphine ligands to form **C1−CO**, the oxidative addition, decarbonylation, and Pd-assisted deprotonation steps were studied (Scheme 7). Coordination of the mixed anhydride to **C1−CO** produces **16** (11.0 kcal mol^{-1}),

DOI: 10.1021/acs.inorgchem.5b02664
Inorg. Chem. 2016, 55, 4124−4131

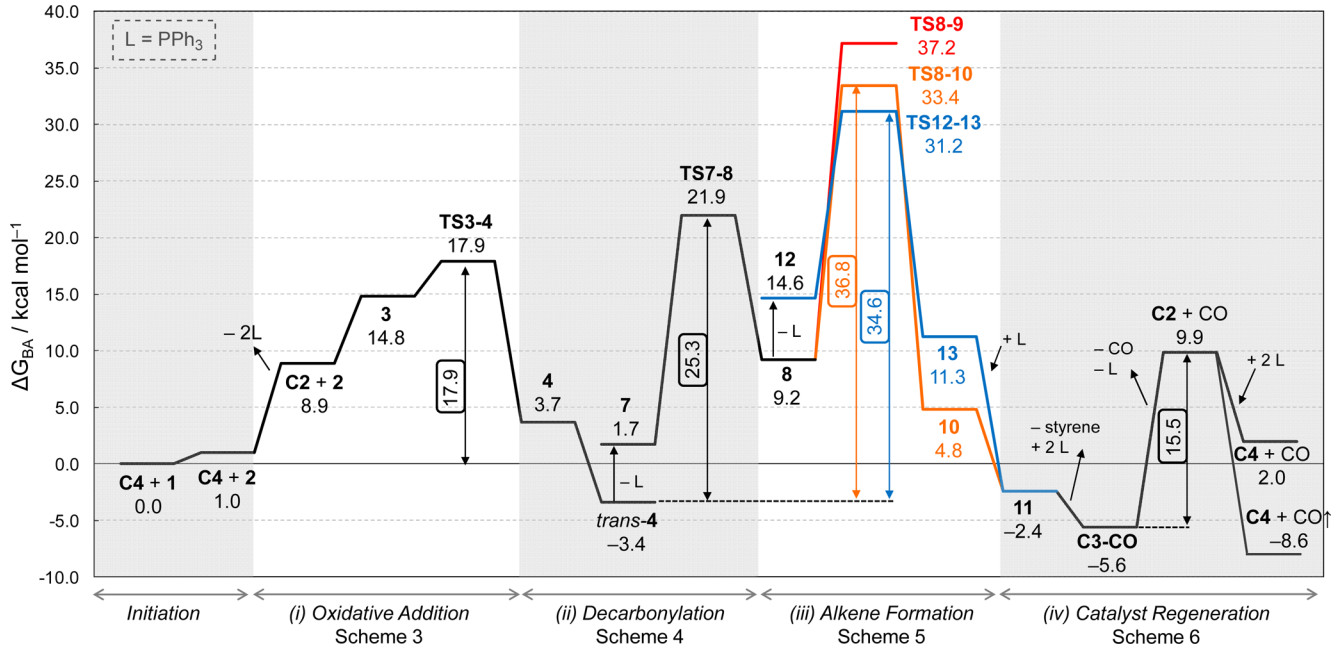

Figure 4. Gibbs free-energy (463.15 K) reaction coordinate for the Pd-catalyzed decarbonylation of hydrocinnamic acid **1**.

Scheme 7. Reaction Mechanism from C3−CO[a]

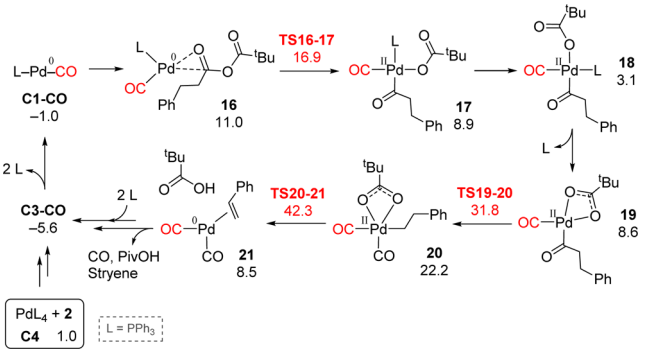

[a] ΔG_{BA} in kcal mol^{-1}.

which then undergoes oxidative addition via **TS16−17** at 16.9 kcal mol^{-1}. **TS16−17** has an energy 1.0 kcal mol^{-1} more stable than that of the previous counterpart **TS3−4** (Scheme 3). The resulting intermediate **17** (8.9 kcal mol^{-1}), which presents CO and PPh_3 in a *cis* position, can isomerize to **18** (3.1 kcal mol^{-1}) with CO and PPh_3 in a *trans* position. Ligand dissociation in **18** forms **19** (8.6 kcal mol^{-1}), from which decarbonylation takes place via **TS19−20** at 31.8 kcal mol^{-1}. Compared to **TS7−8** (Scheme 4), **TS19−20** appears to be 9.9 kcal mol^{-1} less stable. The alkyl intermediate **20** (22.2 kcal mol^{-1}) undergoes a metal-assisted deprotonation via **TS20−21** at an energy of 42.3 kcal mol^{-1}, which is 11.1 kcal mol^{-1} less stable than the analogous transition state **TS12−13** (Scheme 5). Finally, the removal of styrene, pivalic acid, and CO from **21** (8.5 kcal mol^{-1}) and coordination of two phosphine ligands should regenerate the species **C3−CO**.

The Gibbs energy barriers above **C3−CO** for oxidative addition (**TS16−17**), decarbonylation (**TS19−20**), and metal-assisted deprotonation (**TS20−21**) are 22.5, 37.4, and 47.9 kcal mol^{-1}, respectively. We conclude that CO does poison the Pd catalyst, and thus its release is necessary for the reaction to proceed.

Rational Design. In the Pd-catalyzed decarbonylation of hydrocinnamic acid **1**, bis-phosphine (*trans*-**4**) and mono-phosphine (**7**) acyl complexes and monophosphine (**TS8−10**) and phosphine-free (**TS12−13**) metal-assisted deprotonation TS structures have been recognized as the key species that determine the reaction barrier (Figure 4). On that basis, we examine the potential to facilitate the reaction by tuning the anhydride coreactant (and thus the ligand carboxylate group) and/or the phosphine ligands.

Carboxylate Group. Due to the active role of the carboxylate ligand during the metal-assisted deprotonation step (Figure 3), different groups have been computationally evaluated for the key species *trans*-**4** and **TS12−13**, namely, R′ = CH_3 (a), CF_3 (b), Ph (c), *p*-NO_2-Ph (d), and *p*-NMe_2-Ph (e).[56,57] The free energies of corresponding **TS12−13R′** structures relative to the *trans*-**4R′** structures are reported in Scheme 8. As noted above,

Scheme 8. Carboxylate Groups Computationally Tested for the Metal-Assisted Deprotonation Step[a]

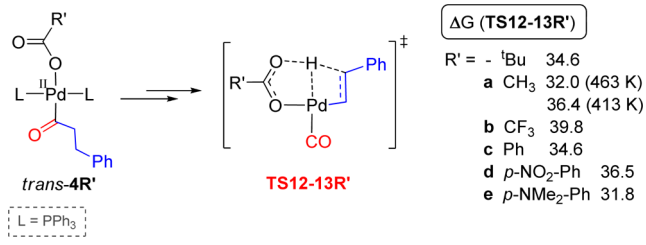

[a] ΔG_{BA} in kcal mol^{-1}.

for R′ = ^{t}Bu, the relevant activation free energy is 34.6 kcal mol^{-1}. When R′ = CH_3, this is slightly decreased to 32.0 kcal mol^{-1}. However, as the boiling point of acetic anhydride is 413.15 K (140 °C), performing the reaction at 463.15 K would require the inconvenience of a sealed reaction vessel. The 413.15 K free energy of activation is 36.4 kcal mol^{-1}, so acetic anhydride is not a particularly attractive alternative. For the strongly electron-withdrawing R′ = CF_3, the reaction becomes

DOI: 10.1021/acs.inorgchem.5b02664
Inorg. Chem. 2016, 55, 4124−4131

less facile, with a computed free energy of activation of 39.8 kcal mol^{-1}. When R′ = Ph, the free energy of activation is 34.6 kcal mol^{-1}, which is not different from the initial R′ = ^{t}Bu alternative. Interestingly, the presence of the electron-withdrawing NO_2 group in the *para* position (σ_p = −0.83[58]) of the benzoate increases the free energy of activation to 36.5 kcal mol^{-1}, whereas the presence of an electron-donating NMe_2 (σ_p = +0.78[58]) decreases it to 31.8 kcal mol^{-1}, indicating the sensitivity of this barrier to overall basicity.

Overall, however, for the R′ groups investigated, no clear correlation was found between the pK_a of their corresponding acids and the free energies of activation,[59] although the Hammett constant σ_p may be useful for correlating phenyl derivatives. This likely reflects some balance in basicity when functioning as a proton abstracting agent and donicity when stabilizing the Pd(II) intermediate. This renders the reaction difficult to improve through manipulation of only this moiety. Of course, the turnover-limiting step *is* the step involving deprotonation, so the only remaining influence is to consider the phosphine ligands, to which we now turn.

Phosphine Ligands. This reaction has been previously tested using several phosphine ligands different from PPh_3, but similar results were obtained.[15] The approach followed herein is focused on the destabilization of the acyl bis-phosphine *trans*-**4** and monophosphine **7** intermediates with respect to the monophosphine **TS8−10** and phosphine-free **TS12−13** transition states. Using PPh_3 as a starting point, we considered the derivatives tri(*o*-tolyl)phosphine (P(*o*-Tol)$_3$, **oT**) and tri(*p*-tolyl)phosphine (P(*p*-Tol)$_3$, **pT**) (Scheme 9). All Gibbs free energies in Scheme 9 are reported with respect to *trans*-**4L** (L = −, **oT**, **pT**).

Scheme 9. Phosphine Ligands Computationally Examined in the Metal-Assisted Deprotonation Step[a]

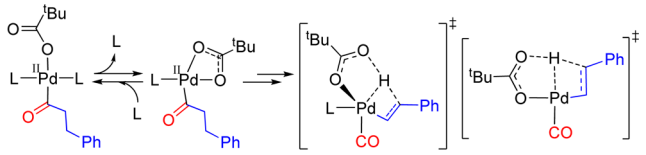

[a] ΔG_{BA} in kcal mol^{-1}.

As noted above for the ligand PPh_3, the monophosphine species **7** is found at an energy 5.1 kcal mol^{-1} above that of *trans*-**4**, and the metal-assisted deprotonation steps have free energies of activation of 36.8 and 34.6 kcal mol^{-1} via **TS8−10** and **TS12−13**, respectively (Figure 4). An examination of the relevant structures shows that **oT** looks promising due to the steric hindrance introduced by the *ortho* methyl groups.[60] Indeed, the monophosphine **7oT** is now isoenergetic with respect to the bis-phosphine *trans*-**4oT**, and the TS structures **TS8−10oT** and **TS12−13** are found at lower energies, 32.0 and 26.0 kcal mol^{-1}, respectively. The estimated free energy of activation using **oT** ligands is 26.0 kcal mol^{-1} from *trans*-**4oT** to **TS12−13** (Scheme 9). Finally, to evaluate the influence of the electronic effect associated with the use of tolyl groups, the less sterically demanding ligand, **pT**, was also considered. The results with **pT** were identical to those of PPh_3 (Scheme 9), suggesting that it is steric hindrance that is responsible for the lower energy barrier found for the **oT** derivatives.

The different number of ligands involved in *trans*-**4L**, **7**, and **TS12−13** (two, one, and none, respectively) permits a more refined tuning of the activation free energy. Overall, the substitution of Ph by the more bulky *o*-Tol provides a decrease in the barrier from 34.6 to 26.0 kcal mol^{-1}. However, while the predicted barrier is lower, a relatively high temperature is still required to exploit entropy to make the dissociation of phosphine ligands more favorable.

CONCLUSIONS

A reaction mechanism has been elucidated for the Pd-catalyzed decarbonylation of hydrocinnamic acid (and by extension, alkylcarboxylic acids in general) via mixed anhydride intermediates. After the initial transformation of the carboxylic acid to the mixed anhydride, the catalytic cycle continues via oxidative addition, decarbonylation, alkene formation, and catalyst regeneration. The turnover-determining step involves the bis-phosphine acyl intermediate *trans*-**4** and the metal-assisted deprotonation TS structure **TS12−13** with an overall Gibbs free energy of activation of 34.6 kcal mol^{-1}. The proposed mechanism also reveals that CO poisons the Pd catalyst. Preliminary studies suggest that the use of bulky phosphine ligands such as P(*o*-Tol)$_3$ may accelerate the reaction significantly; the analogous free energy of activation is predicted to be 26.0 kcal mol^{-1}.

Quantum chemical calculations have helped identify the key intermediates and TS structures involved in the catalytic cycle. The mechanistic insights derived here should help provide a foundation for developing new systems that involve less expensive, earth-abundant transition metals as well as more suitable substrates (e.g., those that avoid the need for sacrificial coreactants). Along these lines, evaluations of analogous reaction mechanisms for Ni derivatives and substrates liable to undergo alkene isomerization are currently underway in our laboratories.

ASSOCIATED CONTENT

Supporting Information

The Supporting Information is available free of charge on the ACS Publications website at DOI: 10.1021/acs.inorgchem.5b02664.

Alternative alkene formation mechanism; Gibbs free-energy reaction coordinate in the gas phase; influence of basis set, solvation during optimization, and density functionals; and energies and Cartesian coordinates of all optimized structures (PDF)

AUTHOR INFORMATION

Corresponding Authors

*E-mail: mortunom@umn.edu.

*E-mail: cramer@umn.edu, Twitter: @ChemProfCramer.

Notes

The authors declare no competing financial interest.

ACKNOWLEDGMENTS

This research was supported by the National Science Foundation (NSF) through the Center for Sustainable Polymers (CHE-1413862). The authors acknowledge the Minnesota Supercomputing Institute (MSI) at the University of Minnesota for providing resources that contributed to the research results reported within this paper.

DOI: 10.1021/acs.inorgchem.5b02664
Inorg. Chem. 2016, 55, 4124−4131

REFERENCES

(1) Dodds, D. R.; Gross, R. *Science* **2007**, *318*, 1250−1251.
(2) Vennestrøm, P. N. R.; Osmundsen, C. M.; Christensen, C. H.; Taarning, E. *Angew. Chem., Int. Ed.* **2011**, *50*, 10502−10509.
(3) Santillan-Jimenez, E.; Crocker, M. *J. Chem. Technol. Biotechnol.* **2012**, *87*, 1041−1050.
(4) Gosselink, R. W.; Hollak, S. A. W.; Chang, S.-W.; van Haveren, J.; de Jong, K. P.; Bitter, J. H.; van Es, D. S. *ChemSusChem* **2013**, *6*, 1576−1594.
(5) Dawes, G. J. S.; Scott, E. L.; Le Nôtre, J.; Sanders, J. P. M.; Bitter, J. H. *Green Chem.* **2015**, *17*, 3231−3250.
(6) Foglia, T. A.; Barr, P. A. *J. Am. Oil Chem. Soc.* **1976**, *53*, 737−741.
(7) For a recent decarboxylation with no coreactants, see: Murray, R. E.; Walter, E. L.; Doll, K. M. *ACS Catal.* **2014**, *4*, 3517−3520.
(8) Goossen, L. J.; Rodríguez, N.; Goossen, K. *Angew. Chem., Int. Ed.* **2008**, *47*, 3100−3120.
(9) (a) Nagayama, K.; Kawataka, F.; Sakamoto, M.; Shimizu, I.; Yamamoto, A. *Chem. Lett.* **1995**, 367−368. (b) Nagayama, K.; Shimizu, I.; Yamamoto, A. *Chem. Lett.* **1998**, 1143−1144. (c) Nagayama, K.; Shimizu, I.; Yamamoto, A. *Bull. Chem. Soc. Jpn.* **2001**, *74*, 1803−1815. (d) Kakino, R.; Narahashi, H.; Shimizu, I.; Yamamoto, A. *Chem. Lett.* **2001**, 1242−1243. (e) Kakino, R.; Narahashi, H.; Shimizu, I.; Yamamoto, A. *Bull. Chem. Soc. Jpn.* **2002**, *75*, 1333−1345.
(10) (a) Goossen, L. J.; Ghosh, K. *Angew. Chem., Int. Ed.* **2001**, *40*, 3458−3460. (b) Goossen, L. J.; Ghosh, K. *Chem. Commun.* **2002**, 836−837. (c) Goossen, L. J.; Winkel, L.; Döhring, A.; Ghosh, K.; Paetzold, J. *Synlett* **2002**, *8*, 1237−1240. (d) Goossen, L. J.; Paetzold, J.; Winkel, L. *Synlett* **2002**, *10*, 1721−1723.
(11) Miller, J. A.; Nelson, J. A.; Byrne, M. P. *J. Org. Chem.* **1993**, *58*, 18−20.
(12) Kraus, G. A.; Riley, S. *Synthesis* **2012**, *44*, 3003−3005.
(13) Goossen, L. J.; Rodríguez, N. *Chem. Commun.* **2004**, 724−725.
(14) Le Nôtre, J.; Scott, E. L.; Franssen, M. C. R.; Sanders, J. P. N. *Tetrahedron Lett.* **2010**, *51*, 3712−3715.
(15) Miranda, M. O.; Pietrangelo, A.; Hillmyer, M. A.; Tolman, W. B. *Green Chem.* **2012**, *14*, 490−494.
(16) Liu, Y.; Kim, K. E.; Herbert, M. B.; Fedorov, A.; Grubbs, R. H.; Stoltz, B. M. *Adv. Synth. Catal.* **2014**, *356*, 130−136.
(17) Liu, Y.; Virgil, S. C.; Grubbs, R. H.; Stoltz, B. M. *Angew. Chem., Int. Ed.* **2015**, *54*, 11800−11804.
(18) Maetani, S.; Fukuyama, T.; Suzuki, N.; Ishihara, D.; Ryu, I. *Chem. Commun.* **2012**, *48*, 2552−2554.
(19) (a) Maetani, S.; Fukuyama, T.; Suzuki, N.; Ishihara, D.; Ryu, I. *Organometallics* **2011**, *30*, 1389−1394. (b) Ternel, J.; Lebarbé, T.; Monflier, E.; Hapiot, F. *ChemSusChem* **2015**, *8*, 1585−1592.
(20) (a) Nagayama, K.; Shimizu, I.; Yamamoto, A. *Bull. Chem. Soc. Jpn.* **1999**, *72*, 799−803. (b) Goossen, L. K.; Paetzold, J. *Angew. Chem., Int. Ed.* **2002**, *41*, 1237−1241.
(21) John, A.; Hogan, L. T.; Hillmyer, M. A.; Tolman, W. B. *Chem. Commun.* **2015**, *51*, 2731−2733.
(22) Sperger, T.; Sanhueza, I. A.; Kalvet, I.; Schoenebeck, F. *Chem. Rev.* **2015**, *115*, 9532−9586.
(23) Cramer, C. J.; Truhlar, D. G. *Phys. Chem. Chem. Phys.* **2009**, *11*, 10757−10816.
(24) Zhao, Y.; Truhlar, D. G. *J. Chem. Phys.* **2006**, *125*, 194101.
(25) (a) Zhao, Y.; Truhlar, D. G. *Acc. Chem. Res.* **2008**, *41*, 157−167. (b) Zhao, Y.; Truhlar, D. G. *Chem. Phys. Lett.* **2011**, *502*, 1−13.
(26) Frisch, M. J.; et al. *Gaussian 09*, revision D.01; Gaussian, Inc.: Wallingford, CT, 2010.
(27) Gusev, D. G. *Organometallics* **2013**, *32*, 4239−4243.
(28) Sieffert, N.; Bühl, M. *Inorg. Chem.* **2009**, *48*, 4622−4624.
(29) Andrae, D.; Haeussermann, U.; Dolg, M.; Stoll, H.; Preuss, H. *Theor. Chim. Acta* **1990**, *77*, 123−141.
(30) (a) Hehre, W. J.; Ditchfield, R.; Pople, J. A. *J. Chem. Phys.* **1972**, *56*, 2257−2261. (b) Francl, M. M.; Pietro, W. J.; Hehre, W. J.; Binkley, J. S.; Gordon, M. S.; DeFrees, D. J.; Pople, J. A. *J. Chem. Phys.* **1982**, *77*, 3654−3665.
(31) Clark, T.; Chandrasekhar, J.; Spitznagel, G. W.; Schleyer, P. *J. Comput. Chem.* **1983**, *4*, 294−301.
(32) Ribeiro, R. F.; Marenich, A. V.; Cramer, C. J.; Truhlar, D. G. *J. Phys. Chem. B* **2011**, *115*, 14556−14562.
(33) *CRC Handbook of Chemistry and Physics*, 95th ed.; Haynes, W. M., Ed.; CRC Press: Boca Raton, FL, 2014−2015.
(34) Ehlers, A. W.; Böhme, M.; Dapprich, S.; Gobbi, A.; Höllwarth, A.; Jonas, V.; Köhler, K. F.; Stegmann, R.; Veldkamp, A.; Frenking, G. *Chem. Phys. Lett.* **1993**, *208*, 111−114.
(35) (a) Krishnan, R.; Binkley, J. S.; Seeger, R.; Pople, J. A. *J. Chem. Phys.* **1980**, *72*, 650−654. (b) McLean, A. D.; Chandler, G. S. *J. Chem. Phys.* **1980**, *72*, 5639−5648.
(36) Marenich, A. V.; Cramer, C. J.; Truhlar, D. G. *J. Phys. Chem. B* **2009**, *113*, 6378−6396.
(37) (a) Riplinger, C.; Neese, F. *J. Chem. Phys.* **2013**, *138*, 034106. (b) Riplinger, C.; Sandhoefer, B.; Hansen, A.; Neese, F. *J. Chem. Phys.* **2013**, *139*, 134101.
(38) Neese, F. *WIREs Comput. Mol. Sci.* **2012**, *2*, 73.
(39) Beletskaya, I. P.; Cheprakov, A. V. *Chem. Rev.* **2000**, *100*, 3009−3066.
(40) Ahlquist, M. S. G.; Norrby, P.-O. *Angew. Chem., Int. Ed.* **2011**, *50*, 11794−11797.
(41) (a) Goossen, L. J.; Koley, D.; Hermann, H. L.; Thiel, W. *J. Am. Chem. Soc.* **2005**, *127*, 11102−11114. (b) Goossen, L. J.; Koley, D.; Hermann, H. L.; Thiel, W. *Organometallics* **2006**, *25*, 54−67.
(42) Ortuño, M. A.; Conejero, S.; Lledós, A. *Beilstein J. Org. Chem.* **2013**, *9*, 1352−1382.
(43) Xie, H.; Sun, Q.; Ren, G.; Cao, Z. *J. Org. Chem.* **2014**, *79*, 11911−11921.
(44) For ester derivatives, see: (a) Li, Z.; Zhang, S.-L.; Fu, Y.; Guo, Q.-X.; Liu, L. *J. Am. Chem. Soc.* **2009**, *131*, 8815−8823. (b) Quasdorf, K. W.; Antoft-Finch, A.; Liu, P.; Silberstein, A. L.; Komaromi, A.; Blackburn, T.; Ramgren, S. D.; Houk, K. N.; Snieckus, V.; Garg, N. K. *J. Am. Chem. Soc.* **2011**, *133*, 6352−6363.
(45) Otsuka, S.; Nakamura, A.; Yoshida, T.; Naruto, M.; Ataka, K. *J. Am. Chem. Soc.* **1973**, *95*, 3180−3188.
(46) A different transition-state structure can be envisaged in which the phosphine ligand L is placed *trans* to the incoming CO. The corresponding transition state **TS7−8′** has an energy 28.1 kcal mol^{-1} above that of the reactants, likely due to the strong *trans* influence of both L and CO ligands.
(47) Because **TS8−9** is not the preferred transition state for alkene formation (see **TS8−10** and **TS12−13** in the main text), the reductive elimination step was not addressed in this study.
(48) A different transition-state structure can be envisaged in which the phosphine ligand L is placed *trans* to the incoming hydride. The corresponding transition state **TS8−9′** is found at an energy 39.8 kcal mol^{-1} above that of the reactants.
(49) Ackermann, L. *Chem. Rev.* **2011**, *111*, 1315−1345.
(50) See, for instance: (a) Davies, D. L.; Donald, S. M. A.; Macgregor, S. A. *J. Am. Chem. Soc.* **2005**, *127*, 13754−13755. (b) Kefalidis, C. E.; Baudoin, O.; Clot, E. *Dalton Trans.* **2010**, *39*, 10528−10535.
(51) Transient $[Pd_n(CO)_m]$ clusters may be present in the solution. See, for instance: (a) Kudo, K.; Hidai, M.; Uchida, Y. *J. Organomet. Chem.* **1971**, *33*, 393−398. (b) Trebbe, R.; Goddard, R.; Rufinska, A.; Seevogel, K.; Pörschke, K.-R. *Organometallics* **1999**, *18*, 2466−2472.
(52) An alternative mechanism to the metal-assisted deprotonation can be proposed assuming that CO is released prior to the alkene formation step (see the Supporting Information for details).
(53) (a) Kozuch, S.; Shaik, S. *Acc. Chem. Res.* **2011**, *44*, 101−110. (b) Kozuch, S.; Martin, J. M. L. *ChemPhysChem* **2011**, *12*, 1413−1418.
(54) Gómez-Gallego, M.; Sierra, M. A. *Chem. Rev.* **2011**, *111*, 4857−4963.
(55) Christensen, N. J.; Fristrup, P. *Synlett* **2015**, *26*, 508−513.
(56) For a systematic comparison of results, butanoic acid is again taken as typical solvent for all calculations. Only small variations are expected in relative energies when using continuum solvation methods.

DOI: 10.1021/acs.inorgchem.5b02664
Inorg. Chem. 2016, 55, 4124−4131

(57) Boutadla, Y.; Davies, D. L.; Macgregor, S. A.; Poblador-Bahamonde, A. I. *Dalton Trans.* **2009**, 5887−5893.
(58) Hansch, C.; Leo, A.; Taft, R. W. *Chem. Rev.* **1991**, *91*, 165−195.
(59) The pK_a values (Gibbs energy barriers at 463.15 K in kcal mol^{-1}) are 4.83 (34.6), 4.56 (32.0), 0.0 (39.8), and 4.0 (34.6) for R′ = ^{t}Bu, CH_3, CF_3, and Ph, respectively. The pK_a values were retrieved from: Appendix 1. In *Applications of Ion Chromatography for Pharmaceutical and Biological Products*, 1st ed.; Bhattacharyya, L., Rohrer, J. S., Eds.; John Wiley & Sons, Inc.: Hoboken, NJ, 2012.
(60) Maleckis, A.; Sanford, M. S. *Organometallics* **2014**, *33*, 3831−3839.

DOI: 10.1021/acs.inorgchem.5b02664
Inorg. Chem. 2016, 55, 4124−4131